3
BUBBLE OR DROPLET TRANSLATION

3.1 INTRODUCTION

In the last chapter it was assumed that the particles were rigid and therefore were not deformed, fissioned or otherwise modified by the flow. However, there are many instances in which the particles that comprise the disperse phase are radically modified by the forces imposed by the continuous phase. Sometimes those modifications are radical enough to, in turn, affect the flow of the continuous phase. For example, the shear rates in the continuous phase may be sufficient to cause fission of the particles and this, in turn, may reduce the relative motion and therefore alter the global extent of phase separation in the flow.

The purpose of this chapter is to identify additional phenomena and issues that arise when the translating disperse phase consists of deformable *particles*, namely bubbles, droplets or fissionable solid grains.

3.2 DEFORMATION DUE TO TRANSLATION

3.2.1 Dimensional analysis

Since the fluid stresses due to translation may deform the bubbles, drops or deformable solid particles that make up the disperse phase, we should consider not only the parameters governing the deformation but also the consequences in terms of the translation velocity and the shape. We concentrate here on bubbles and drops in which surface tension, S, acts as the force restraining deformation. However, the reader will realize that there would exist a similar analysis for deformable elastic particles. Furthermore, the discussion will be limited to the case of *steady* translation, caused by gravity, g. Clearly the results could be extended to cover translation due

to fluid acceleration by using an effective value of g as indicated in section 2.4.2.

The characteristic force maintaining the sphericity of the bubble or drop is given by SR. Deformation will occur when the characteristic anisotropy in the fluid forces approaches SR; the magnitude of the anisotropic fluid force will be given by $\mu_L W_\infty R$ for $W_\infty R/\nu_L \ll 1$ or by $\rho_L W_\infty^2 R^2$ for $W_\infty R/\nu_L \gg 1$. Thus defining a Weber number, $We = 2\rho_L W_\infty^2 R/S$, deformation will occur when We/Re approaches unity for $Re \ll 1$ or when We approaches unity for $Re \gg 1$. But evaluation of these parameters requires knowledge of the terminal velocity, W_∞, and this may also be a function of the shape. Thus one must start by expanding the functional relation of equation 2.87 which determines W_∞ to include the Weber number:

$$F(Re, We, Fr) = 0 \tag{3.1}$$

This relation determines W_∞ where Fr is given by equations 2.85. Since all three dimensionless coefficients in this functional relation include both W_∞ and R, it is simpler to rearrange the arguments by defining another nondimensional parameter, the Haberman-Morton number (1953), Hm, that is a combination of We, Re, and Fr but does not involve W_∞. The Haberman-Morton number is defined as

$$Hm = \frac{We^3}{Fr^2 Re^4} = \frac{g\mu_L^4}{\rho_L S^3}\left(1 - \frac{m_p}{\rho_L v}\right) \tag{3.2}$$

In the case of a bubble, $m_p \ll \rho_L v$ and therefore the factor in parenthesis is usually omitted. Then Hm becomes independent of the bubble size. It follows that the terminal velocity of a bubble or drop can be represented by functional relation

$$F(Re, Hm, Fr) = 0 \quad \text{or} \quad F^*(Re, Hm, C_D) = 0 \tag{3.3}$$

and we shall confine the following discussion to the nature of this relation for bubbles ($m_p \ll \rho_L v$).

Some values for the Haberman-Morton number (with $m_p/\rho_L v = 0$) for various saturated liquids are shown in figure 3.1; other values are listed in table 3.1. Note that for all but the most viscous liquids, Hm is much less than unity. It is, of course, possible to have fluid accelerations much larger than g; however, this is unlikely to cause Hm values greater than unity in practical multiphase flows of most liquids.

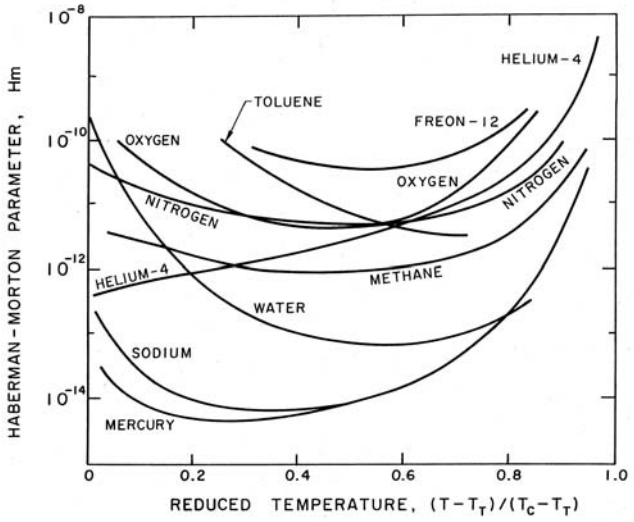

Figure 3.1. Values of the Haberman-Morton parameter, Hm, for various pure substances as a function of reduced temperature where T_T is the triple point temperature and T_C is the critical point temperature.

Table 3.1. *Values of the Haberman-Morton numbers, $Hm = g\mu_L^4/\rho_L S^3$, for various liquids at normal temperatures.*

Filtered Water	0.25×10^{-10}	Turpentine	2.41×10^{-9}
Methyl Alcohol	0.89×10^{-10}	Olive Oil	7.16×10^{-3}
Mineral Oil	1.45×10^{-2}	Syrup	0.92×10^{6}

3.2.2 Bubble shapes and terminal velocities

Having introduced the Haberman-Morton number, we can now identify the conditions for departure from sphericity. For low Reynolds numbers ($Re \ll 1$) the terminal velocity will be given by $Re \propto Fr^2$. Then the shape will deviate from spherical when $We \geq Re$ or, using $Re \propto Fr^2$ and $Hm = We^3 Fr^{-2} Re^{-4}$, when

$$Re \geq Hm^{-\frac{1}{2}} \tag{3.4}$$

Thus if $Hm < 1$ all bubbles for which $Re \ll 1$ will remain spherical. However, there are some unusual circumstances in which $Hm > 1$ and then there will be a range of Re, namely $Hm^{-\frac{1}{2}} < Re < 1$, in which significant departure from sphericity might occur.

For high Reynolds numbers ($Re \gg 1$) the terminal velocity is given by $Fr \approx O(1)$ and distortion will occur if $We > 1$. Using $Fr = 1$ and $Hm = We^3 Fr^{-2} Re^{-4}$ it follows that departure from sphericity will occur when

$$Re \gg Hm^{-\frac{1}{4}} \tag{3.5}$$

Consequently, in the common circumstances in which $Hm < 1$, there exists a range of Reynolds numbers, $Re < Hm^{-\frac{1}{4}}$, in which sphericity is maintained; nonspherical shapes occur when $Re > Hm^{-\frac{1}{4}}$. For $Hm > 1$ departure from sphericity has already occurred at $Re < 1$ as discussed above.

Experimentally, it is observed that the initial departure from sphericity causes ellipsoidal bubbles that may oscillate in shape and have oscillatory trajectories (Hartunian and Sears 1957). As the bubble size is further increased to the point at which $We \approx 20$, the bubble acquires a new asymptotic shape, known as a *spherical-cap bubble.* A photograph of a typical spherical-cap bubble is shown in figure 3.2; the notation used to describe the approximate geometry of these bubbles is sketched in the same figure. Spherical-cap bubbles were first investigated by Davies and Taylor (1950), who observed that the terminal velocity is simply related to the radius of curvature of the cap, R_C, or to the equivalent volumetric radius, R_B, by

$$W_\infty = \frac{2}{3}(gR_C)^{\frac{1}{2}} = (gR_B)^{\frac{1}{2}} \tag{3.6}$$

Assuming a typical laminar drag coefficient of $C_D = 0.5$, a spherical solid particle with the same volume would have a terminal velocity,

$$W_\infty = (8gR_B/3C_D)^{\frac{1}{2}} = 2.3(gR_B)^{\frac{1}{2}} \tag{3.7}$$

that is substantially higher than the spherical-cap bubble. From equation 3.6 it follows that the effective C_D for spherical-cap bubbles is 2.67 based on the area πR_B^2.

Wegener and Parlange (1973) have reviewed the literature on spherical-cap bubbles. Figure 3.3 is taken from their review and shows that the value of $W_\infty/(gR_B)^{\frac{1}{2}}$ reaches a value of about 1 at a Reynolds number, $Re = 2W_\infty R_B/\nu_L$, of about 200 and, thereafter, remains fairly constant. Visualization of the flow reveals that, for Reynolds numbers less than about 360, the wake behind the bubble is laminar and takes the form of a toroidal vortex (similar to a Hill (1894) spherical vortex) shown in the left-hand photograph of figure 3.4. The wake undergoes transition to turbulence about $Re = 360$, and bubbles at higher Re have turbulent wakes as illustrated in the right side of figure 3.4. We should add that scuba divers have long observed that spherical-cap bubbles rising in the ocean seem to have a max-

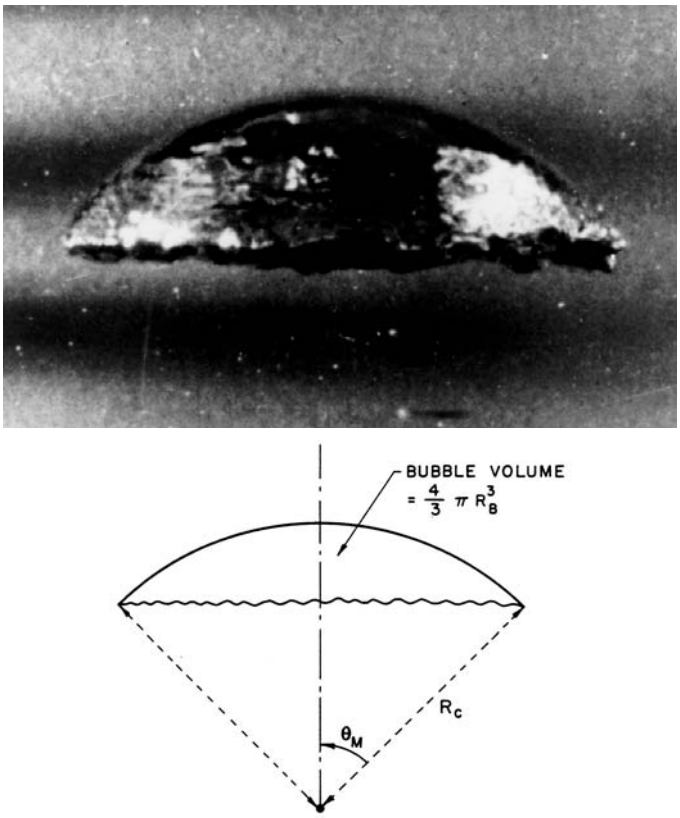

Figure 3.2. Photograph of a spherical cap bubble rising in water (from Davenport, Bradshaw, and Richardson 1967) with the notation used to describe the geometry of spherical cap bubbles.

imum size of the order of 30 cm in diameter. When they grow larger than this, they fission into two (or more) bubbles. However, the author has found no quantitative study of this fission process.

In closing, we note that the terminal velocities of the bubbles discussed here may be represented according to the functional relation of equations 3.3 as a family of $C_D(Re)$ curves for various Hm. Figure 3.5 has been extracted from the experimental data of Haberman and Morton (1953) and shows the dependence of $C_D(Re)$ on Hm at intermediate Re. The curves cover the spectrum from the low Re spherical bubbles to the high Re spherical cap bubbles. The data demonstrate that, at higher values of Hm, the drag coefficient makes a relatively smooth transition from the low Reynolds number result to the spherical cap value of about 2.7. Lower values of Hm result in

a deep minimum in the drag coefficient around a Reynolds number of about 200.

3.3 MARANGONI EFFECTS

Even if a bubble remains quite spherical, it can experience forces due to gradients in the surface tension, S, over the surface that modify the surface boundary conditions and therefore the translational velocity. These are called Marangoni effects. The gradients in the surface tension can be caused by a number of different factors. For example, gradients in the temperature, solvent concentration, or electric potential can create gradients in the surface tension. The *thermocapillary* effects due to temperature gradients have been

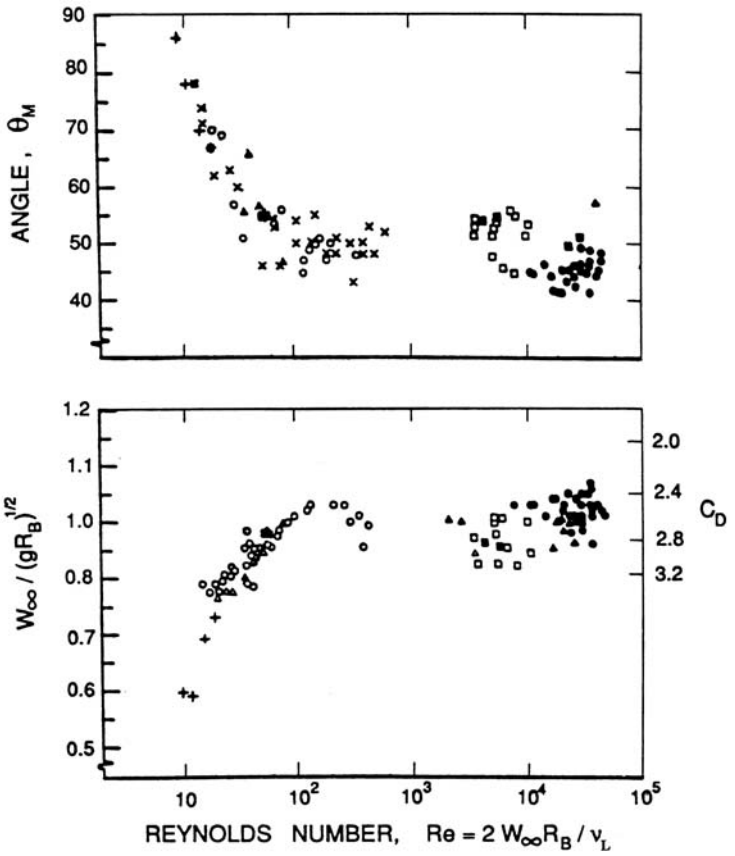

Figure 3.3. Data on the terminal velocity, $W_\infty/(gR_B)^{\frac{1}{2}}$, and the conical angle, θ_M, for spherical-cap bubbles studied by a number of different investigators (adapted from Wegener and Parlange 1973).

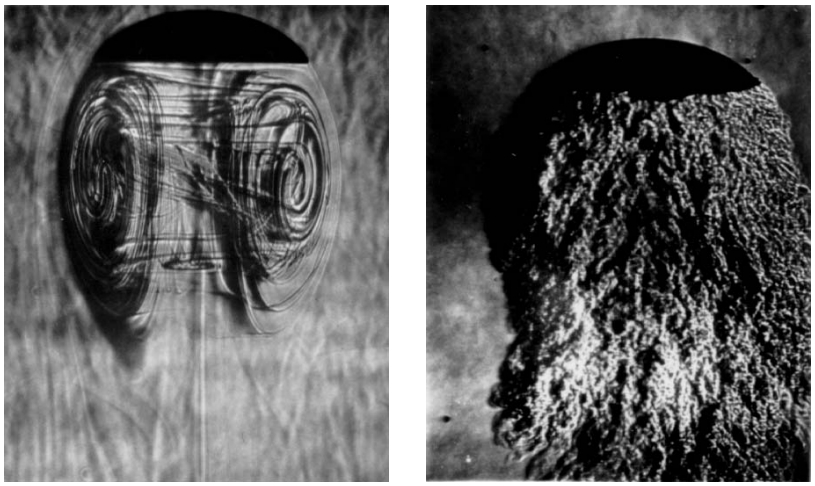

Figure 3.4. Flow visualizations of spherical-cap bubbles. On the left is a bubble with a laminar wake at $Re \approx 180$ (from Wegener and Parlange 1973) and, on the right, a bubble with a turbulent wake at $Re \approx 17,000$ (from Wegener, Sundell and Parlange 1971, reproduced with permission of the authors).

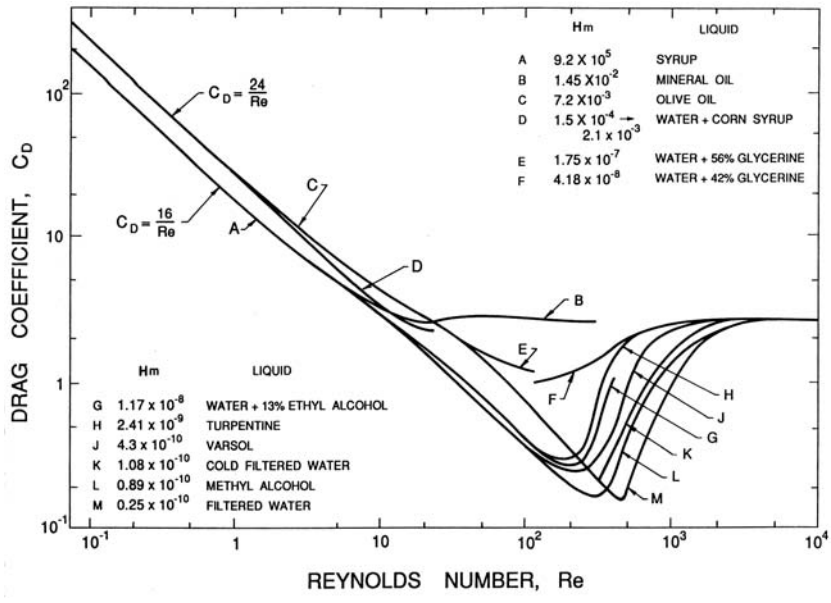

Figure 3.5. Drag coefficients, C_D, for bubbles as a function of the Reynolds number, Re, for a range of Haberman-Morton numbers, Hm, as shown. Data from Haberman and Morton (1953).

explored by a number of investigators (for example, Young, Goldstein, and Block 1959) because of their importance in several technological contexts. For most of the range of temperatures, the surface tension decreases linearly with temperature, reaching zero at the critical point. Consequently, the controlling thermophysical property, dS/dT, is readily identified and more or less constant for any given fluid. Some typical data for dS/dT is presented in table 3.2 and reveals a remarkably uniform value for this quantity for a wide range of liquids.

Surface tension gradients affect free surface flows because a gradient, dS/ds, in a direction, s, tangential to a surface clearly requires that a shear stress act in the negative s direction in order that the surface be in equilibrium. Such a shear stress would then modify the boundary conditions (for example, the Hadamard-Rybczynski conditions used in section 2.2.2), thus altering the flow and the forces acting on the bubble.

As an example of the Marangoni effect, we will examine the steady motion of a spherical bubble in a viscous fluid when there exists a gradient of the temperature (or other controlling physical property), dT/dx_1, in the direction of motion (see figure 2.1). We must first determine whether the temperature (or other controlling property) is affected by the flow. It is illustrative to consider two special cases from a spectrum of possibilities. The first and simplest special case, that is not so relevant to the thermocapillary phenomenon, is to assume that $T = (dT/dx_1)x_1$ throughout the flow field so that, on the surface of the bubble,

$$\left(\frac{1}{R}\frac{dS}{d\theta}\right)_{r=R} = -\sin\theta\left(\frac{dS}{dT}\right)\left(\frac{dT}{dx_1}\right) \tag{3.8}$$

Much more realistic is the assumption that thermal conduction dominates the heat transfer ($\nabla^2 T = 0$) and that there is no heat transfer through the surface of the bubble. Then it follows from the solution of Laplace's equation for the conductive heat transfer problem that

$$\left(\frac{1}{R}\frac{dS}{d\theta}\right)_{r=R} = -\frac{3}{2}\sin\theta\left(\frac{dS}{dT}\right)\left(\frac{dT}{dx_1}\right) \tag{3.9}$$

The latter is the solution presented by Young, Goldstein, and Block (1959), but it differs from equation 3.8 only in terms of the effective value of dS/dT. Here we shall employ equation 3.9 since we focus on thermocapillarity, but other possibilities such as equation 3.8 should be borne in mind.

For simplicity we will continue to assume that the bubble remains spherical. This assumption implies that the surface tension differences are small

Table 3.2. *Values of the temperature gradient of the surface tension, $-dS/dT$, for pure liquid/vapor interfaces (in $kg/s^2\ K$).*

Water	2.02×10^{-4}	Methane	1.84×10^{-4}
Hydrogen	1.59×10^{-4}	Butane	1.06×10^{-4}
Helium-4	1.02×10^{-4}	Carbon Dioxide	1.84×10^{-4}
Nitrogen	1.92×10^{-4}	Ammonia	1.85×10^{-4}
Oxygen	1.92×10^{-4}	Toluene	0.93×10^{-4}
Sodium	0.90×10^{-4}	Freon-12	1.18×10^{-4}
Mercury	3.85×10^{-4}	Uranium Dioxide	1.11×10^{-4}

compared with the absolute level of S and that the stresses normal to the surface are entirely dominated by the surface tension.

With these assumptions the tangential stress boundary condition for the spherical bubble becomes

$$\rho_L \nu_L \left(\frac{\partial u_\theta}{\partial r} - \frac{u_\theta}{r} \right)_{r=R} + \frac{1}{R} \left(\frac{dS}{d\theta} \right)_{r=R} = 0 \tag{3.10}$$

and this should replace the Hadamard-Rybczynski condition of zero shear stress that was used in section 2.2.2. Applying the boundary condition given by equations 3.10 and 3.9 (as well as the usual kinematic condition, $(u_r)_{r=R} = 0$) to the low Reynolds number solution given by equations 2.11, 2.12 and 2.13 leads to

$$A = -\frac{R^4}{4\rho_L \nu_L} \frac{dS}{dx_1} \quad ; \quad B = \frac{WR}{2} + \frac{R^2}{4\rho_L \nu_L} \frac{dS}{dx_1} \tag{3.11}$$

and consequently, from equation 2.14, the force acting on the bubble becomes

$$F_1 = -4\pi \rho_L \nu_L W R - 2\pi R^2 \frac{dS}{dx_1} \tag{3.12}$$

In addition to the normal Hadamard-Rybczynski drag (first term), we can identify a Marangoni force, $2\pi R^2 (dS/dx_1)$, acting on the bubble in the direction of *decreasing* surface tension. Thus, for example, the presence of a uniform temperature gradient, dT/dx_1, would lead to an additional force on the bubble of magnitude $2\pi R^2 (-dS/dT)(dT/dx_1)$ in the direction of the warmer fluid since the surface tension decreases with temperature. Such thermocapillary effects have been observed and measured by Young, Goldstein, and Block (1959) and others.

Finally, we should comment on a related effect caused by surface contam-

inants that increase the surface tension. When a bubble is moving through liquid under the action, say, of gravity, convection may cause contaminants to accumulate on the downstream side of the bubble. This will create a positive $dS/d\theta$ gradient that, in turn, will generate an effective shear stress acting in a direction opposite to the flow. Consequently, the contaminants tend to immobilize the surface. This will cause the flow and the drag to change from the Hadamard-Rybczynski solution to the Stokes solution for zero tangential velocity. The effect is more pronounced for smaller bubbles since, for a given surface tension difference, the Marangoni force becomes larger relative to the buoyancy force as the bubble size decreases. Experimentally, this means that surface contamination usually results in Stokes drag for spherical bubbles smaller than a certain size and in Hadamard-Rybczynski drag for spherical bubbles larger than that size. Such a transition is observed in experiments measuring the rise velocity of bubbles and can be see in the data of Haberman and Morton (1953) included as figure 3.5. Harper, Moore, and Pearson (1967) have analyzed the more complex hydrodynamic case of higher Reynolds numbers.

3.4 BJERKNES FORCES

Another force that can be important for bubbles is that experienced by a bubble placed in an acoustic field. Termed the Bjerknes force, this non-linear effect results from the the finite wavelength of the sound waves in the liquid. The frequency, wavenumber, and propagation speed of the stationary acoustic field will be denoted by ω, κ and c_L respectively where $\kappa = \omega/c_L$. The finite wavelength implies an instantaneous pressure gradient in the liquid and, therefore, a *buoyancy* force acting on the bubble.

To model this we express the instantaneous pressure, p by

$$p = p_o + Re\{\tilde{p}^* \sin(\kappa x_i) e^{i\omega t}\} \tag{3.13}$$

where p_o is the mean pressure level, $\tilde{p}^*$ is the amplitude of the sound waves and x_i is the direction of wave propagation. Like any other pressure gradient, this produces an instantaneous force, F_i, on the bubble in the x_i direction given by

$$F_i = -\frac{4}{3}\pi R^3 \left(\frac{dp}{dx_i}\right) \tag{3.14}$$

where R is the instantaneous radius of the spherical bubble. Since both R and dp/dx_i contain oscillating components, it follows that the combination of these in equation 3.14 will lead to a nonlinear, time-averaged component

in F_i, that we will denote by $\bar{F}_i$. Expressing the oscillations in the volume or radius by

$$R = R_e \left[1 + Re\{\varphi e^{i\omega t}\}\right] \tag{3.15}$$

one can use the Rayleigh-Plesset equation (see section 4.2.1) to relate the pressure and radius oscillations and thus obtain

$$Re\{\varphi\} = \frac{\tilde{p}^*(\omega^2 - \omega_n^2)\sin(\kappa x_i)}{\rho_L R_e^2 \left[(\omega^2 - \omega_n^2)^2 + (4\nu_L\omega/R_e^2)^2\right]} \tag{3.16}$$

where ω_n is the natural frequency of volume oscillation of an individual bubble (see section 4.4.1) and μ_L is the effective viscosity of the liquid in damping the volume oscillations. If ω is not too close to ω_n, a useful approximation is

$$Re\{\varphi\} \approx \tilde{p}^* \sin(\kappa x_i)/\rho_L R_e^2(\omega^2 - \omega_n^2) \tag{3.17}$$

Finally, substituting equations 3.13, 3.15, 3.16, and 3.17 into 3.14 one obtains

$$\bar{F}_i = -2\pi R_e^3 Re\{\varphi\}\kappa\tilde{p}^* \cos(\kappa x_i) \approx -\frac{\pi\kappa R_e(\tilde{p}^*)^2 \sin(2\kappa x_i)}{\rho_L(\omega^2 - \omega_n^2)} \tag{3.18}$$

This is known as the primary Bjerknes force since it follows from some of the effects discussed by that author (Bjerknes 1909). The effect was first properly identified by Blake (1949).

The form of the primary Bjerknes force produces some interesting bubble migration patterns in a stationary sound field. Note from equation (3.18) that if the excitation frequency, ω, is less than the bubble natural frequency, ω_n, then the primary Bjerknes force will cause migration of the bubbles away from the nodes in the pressure field and toward the antinodes (points of largest pressure amplitude). On the other hand, if $\omega > \omega_n$ the bubbles will tend to migrate from the antinodes to the nodes. A number of investigators (for example, Crum and Eller 1970) have observed the process by which small bubbles in a stationary sound field first migrate to the antinodes, where they grow by rectified diffusion (see section 4.4.3) until they are larger than the resonant radius. They then migrate back to the nodes, where they may dissolve again when they experience only small pressure oscillations. Crum and Eller (1970) and have shown that the translational velocities of migrating bubbles are compatible with the Bjerknes force estimates given above.

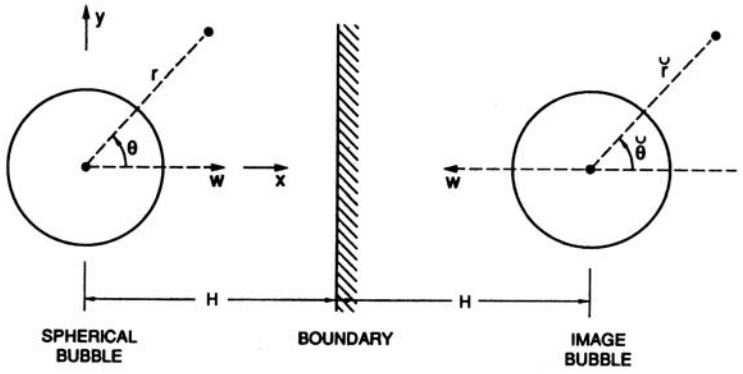

Figure 3.6. Schematic of a bubble undergoing growth or collapse close to a plane boundary. The associated translational velocity is denoted by W.

3.5 GROWING OR COLLAPSING BUBBLES

When the volume of a bubble changes significantly, that growth or collapse can also have a substantial effect upon its translation. In this section we return to the discussion of high Re flow in section 2.3.3 and specifically address the effects due to bubble growth or collapse. A bubble that grows or collapses close to a boundary may undergo translation due to the asymmetry induced by that boundary. A relatively simple example of the analysis of this class of flows is the case of the growth or collapse of a spherical bubble near a plane boundary, a problem first solved by Herring (1941) (see also Davies and Taylor 1942, 1943). Assuming that the only translational motion of the bubble is perpendicular to the plane boundary with velocity, W, the geometry of the bubble and its image in the boundary will be as shown in figure 3.6. For convenience, we define additional polar coordinates, $(\breve{r}, \breve{\theta})$, with origin at the center of the image bubble. Assuming inviscid, irrotational flow, Herring (1941) and Davies and Taylor (1943) constructed the velocity potential, ϕ, near the bubble by considering an expansion in terms of R/H where H is the distance of the bubble center from the boundary. Neglecting all terms that are of order R^3/H^3 or higher, the velocity potential can be obtained by superimposing the individual contributions from the bubble source/sink, the image source/sink, the bubble translation dipole, the image dipole, and one correction factor described below. This combination yields

$$\phi = -\frac{R^2\dot{R}}{r} - \frac{WR^3\cos\theta}{2r^2} \pm \left\{ -\frac{R^2\dot{R}}{\breve{r}} + \frac{WR^3\cos\breve{\theta}}{2\breve{r}^2} - \frac{R^5\dot{R}\cos\theta}{8H^2r^2} \right\} \quad (3.19)$$

The first and third terms are the source/sink contributions from the bubble and the image respectively. The second and fourth terms are the dipole contributions due to the translation of the bubble and the image. The last term arises because the source/sink in the bubble needs to be displaced from the bubble center by an amount $R^3/8H^2$ normal to the wall in order to satisfy the boundary condition on the surface of the bubble to order R^2/H^2. All other terms of order R^3/H^3 or higher are neglected in this analysis assuming that the bubble is sufficiently far from the boundary so that $H \gg R$. Finally, the sign choice on the last three terms of equation 3.19 is as follows: the upper, positive sign pertains to the case of a solid boundary and the lower, negative sign provides an approximate solution for a free surface boundary.

It remains to use this solution to determine the translational motion, $W(t)$, normal to the boundary. This is accomplished by invoking the condition that there is no net force on the bubble. Using the unsteady Bernoulli equation and the velocity potential and fluid velocities obtained from equation (3.19), Davies and Taylor (1943) evaluate the pressure at the bubble surface and thereby obtain an expression for the force, F_x, on the bubble in the x direction:

$$F_x = -\frac{2\pi}{3}\left\{\frac{d}{dt}\left(R^3 W\right) \pm \frac{3}{4}\frac{R^2}{H^2}\frac{d}{dt}\left(R^3\frac{dR}{dt}\right)\right\} \tag{3.20}$$

Adding the effect of buoyancy due to a component, g_x, of the gravitational acceleration in the x direction, Davies and Taylor then set the total force equal to zero and obtain the following equation of motion for $W(t)$:

$$\frac{d}{dt}\left(R^3 W\right) \pm \frac{3}{4}\frac{R^2}{H^2}\frac{d}{dt}\left(R^3\frac{dR}{dt}\right) + \frac{4\pi R^3 g_x}{3} = 0 \tag{3.21}$$

In the absence of gravity this corresponds to the equation of motion first obtained by Herring (1941). Many of the studies of growing and collapsing bubbles near boundaries have been carried out in the context of underwater explosions (see Cole 1948). An example illustrating the solution of equation 3.21 and the comparison with experimental data is included in figure 3.7 taken from Davies and Taylor (1943).

Another application of this analysis is to the translation of cavitation bubbles near walls. Here the motivation is to understand the development of impulsive loads on the solid surface. Therefore the primary focus is on bubbles close to the wall and the solution described above is of limited value since it requires $H \gg R$. However, considerable progress has been made in recent years in developing analytical methods for the solution of the inviscid

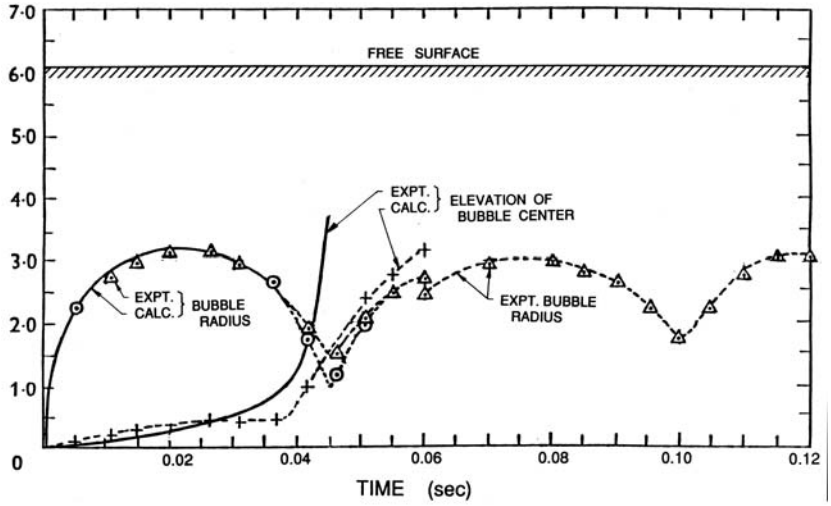

Figure 3.7. Data from Davies and Taylor (1943) on the mean radius and central elevation of a bubble in oil generated by a spark-initiated explosion of 1.32×10^6 *ergs* situated 6.05 *cm* below the free surface. The two measures of the bubble radius are one half of the horizontal span ($\triangle$) and one quarter of the sum of the horizontal and vertical spans ($\odot$). Theoretical calculations using Equation (3.21) are indicated by the solid lines.

free surface flows of bubbles near boundaries (Blake and Gibson 1987). One of the concepts that is particularly useful in determining the direction of bubble translation is based on a property of the flow first introduced by Kelvin (see Lamb 1932) and called the Kelvin impulse. This vector property applies to the flow generated by a finite particle or bubble in a fluid; it is denoted by I_{Ki} and defined by

$$I_{Ki} = \rho_L \int_{S_B} \phi n_i dS \tag{3.22}$$

where ϕ is the velocity potential of the irrotational flow, S_B is the surface of the bubble, and n_i is the outward normal at that surface (defined as positive into the bubble). If one visualizes a bubble in a fluid at rest, then the Kelvin impulse is the impulse that would have to be applied to the bubble in order to generate the motions of the fluid related to the bubble motion. Benjamin and Ellis (1966) were the first to demonstrate the value of this property in determining the interaction between a growing or collapsing bubble and a nearby boundary (see also Blake and Gibson 1987).